Multi-objective Optimization Design of Inset-surface Permanent Magnet Machine Considering Deterministic and Robust Performances*

Gaohong Xu, *Zexin Jia*, *Wenxiang Zhao**, *Qian Chen and Guohai Liu*
(School of Electrical and Information Engineering, Jiangsu University, Zhenjiang 212013, China)

Abstract: The inset-surface permanent magnet (ISPM) machine can achieve the desired electromagnetic performance according to the traditional deterministic design. However, the reliability and quality of the machine may be affected by the essential manufacturing tolerances and unavoidable noise factors in mass production. To address this weakness, a comprehensive multi-objective optimization design method is proposed, in which robust optimization is performed after the deterministic design. The response surface method is first adopted to establish the optimization objective equation. Afterward, the sample points are obtained via Monte Carlo simulation considering the design-variable uncertainty. The Design for Six Sigma approach is adopted to ensure the robustness of the design model. Furthermore, the barebones multi-objective particle swarm optimization algorithm is used to obtain a compromise solution. A prototype is manufactured to evaluate the effectiveness of the proposed method. According to the finite-element analysis and experimental tests, the electromagnetic performance and reliability of the machine are significantly enhanced with the proposed method.

Keywords: Multi-objective optimization design, robust design, Design for Six Sigma, Monte Carlo simulation, barebones multi-objective particle swarm optimization

1 Introduction

Inset-surface permanent magnet (ISPM) machines have been successfully used in various applications, such as electric vehicles, wind power generation, and shift propulsion [1-4], due to their high efficiency, high torque density, and good weakening capability [5-7]. However, owing to the concavity and convexity of the machine structure and the coupling effect of the magnetic field, ISPM machines suffer from undesirable torque ripple. For improving the electromagnetic performance, numerous design methods have been investigated. Rotor magnet shifting and asymmetric rotor shape techniques are effective for torque-ripple reduction [8-10]. However, these methods are only suitable for an even number of rotor teeth or rotor magnets. For obtaining a sufficient average torque, air barriers are introduced into the machine to compensate for the reduction in the average torque with a significant torque-ripple reduction [11-12], which reduces the overall rotational stability of the rotor and causes large amounts of vibration and noise. Additionally, the third harmonic current is injected for producing an extra torque to counteract the torque ripple [13]. However, this makes the control system more complex. Thus, to obtain a high average torque and low torque ripple simultaneously, the tradeoffs between different design variables and objectives should be considered.

Among the multi-objective optimization design methods, the fuzzy-based Taguchi method is a classic technique for multi-objective optimization design [14-15]. Although the torque performance can be enhanced, the number of optimization objectives is limited, and the combinations of design variables are restricted. Moreover, this method can only be used to solve the

Manuscript received March 31, 2021; revised May 6, 2021; accepted July 20, 2021. Date of publication September 30, 2021; date of current version August 11, 2021.
* Corresponding Author, E-mail: zwx@ujs.edu.cn
* Supported by the National Natural Science Foundation of China (51907080), by the Natural Science Foundation of Jiangsu Province (BK20190848), and by the China Postdoctoral Science Foundation (2019M661746).
Digital Object Identifier: 10.23919/CJEE.2021.000027

single-objective problem and has drawbacks for solving multi-objective optimization problems. Recently, numerous intelligent optimization algorithms, e.g., multi-objective differential evolution with a ranking-based mutation operator, sequential nonlinear programming, and genetic algorithms, have been successfully applied in deterministic design [16-18], exhibiting high accuracy and efficiency. Although the electromagnetic performance can be significantly improved by appropriate optimization algorithms, the noise factors, such as uncontrollable manufacturing tolerances of design variables, deviations in material characteristics, and imperfections in assembly, are inevitable (particularly in mass production), resulting in perturbations to the electromagnetic performance and affecting the reliability and manufacturing cost of the machine [19]. Therefore, it is vital to adopt robust optimization design to reduce the sensitivity of design variables, which is challenging for most machines.

Given that the manufacturing tolerances and material characteristic variations cause additional harmonics in the cogging torque [20-23], Ref. [23] provided detailed theoretical and experimental analyses concerning the frequency-spectrum components of the cogging torque caused by the manufacturing tolerances of the stator and rotor. Rotation lamination is proposed for manufacturing the stator and rotor stacks. However, the stamping efficiency is reduced because of the rotation requirement. Furthermore, most studies have focused on single-objective optimization design. With the strict requirements of the machine, multiple objectives must be considered simultaneously. When a single-objective optimization design is adopted, a large amount of computation is needed, which is time-consuming. Thus, a multi-objective optimization design is needed. Probabilistic design approaches, Design for Six Sigma (DFSS), and Monte Carlo simulation (MCS) are widely used techniques for multi-objective robust optimization design [24-25]. MCS can effectively estimate the mean and standard deviations in a robust optimization model by using random sampling statistics. Afterward, DFSS is employed to establish a robust optimization equation considering the manufacturing tolerances, which can satisfy the short- and long-term design requirements [26].

This paper proposes a comprehensive multi-objective optimization method that can not only efficiently determine the appropriate values of the design variables but also consider the unavoidable noise factors, which can significantly reduce the product defect rate during mass production. The remainder of this paper is organized as follows. The ISPM motor structure and design specifications are presented in Section 2. Then, in Section 3, the multi-objective deterministic optimization design is developed by using multi-level design and the barebones multi-objective particle swarm optimization (BB-MOPSO) algorithm. The robust optimization process involving DFSS and MCS is described in Section 4. Verification of the robustness is presented in Section 5. The machine was manufactured and tested to verify the effectiveness of the proposed method, as described in Section 6. Finally, conclusions are drawn in Section 7.

2 Machine topology and design specifications

2.1 Machine topology

The number of periods plays an important role in torque ripple. When the number of slots per phase and per pole and the number of poles are the same, the number of torque-ripple periods in the five-phase machine is larger than that for the three-phase machine [27]. Therefore, the five-phase, 80-slot, and 8-pole ISPM machine is selected to reduce the torque ripple.

Shifting the rotor magnets can suppress the torque ripple by generating an angular difference of the electromagnetic torque between the shifted and non-shifted magnetic poles [8]. Thus, the rotor magnets are shifted twice in this study. First, the two magnetic poles (M1, M2) and (M5, M6) are viewed as basic units and shifted by SW1. Afterward, four magnetic poles (M1, M2, M3, M4) are viewed as basic units and shifted by SW2. The torque ripple can be significantly reduced, and torque loss is inevitable. Thus, the assisted air barriers are added to compensate for the torque loss by shifting the magnetoresistive torque angle. Moreover, the design variables are increased. The configuration of the proposed machine is shown in Fig. 1, and the parametric model is presented in Fig. 2.

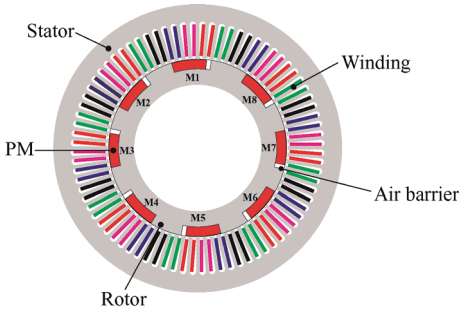

Fig. 1 Configuration of the ISPM machine

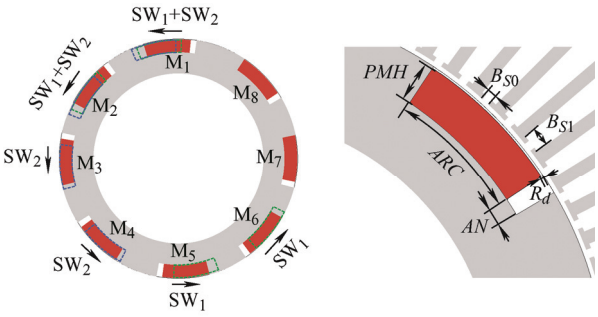

(a) Rotor magnet shift angles (b) Optimization variables

Fig. 2 Parametric model of the ISPM machine

2.2 Design specifications

Tab. 1 presents the design specifications. The initial values and variation ranges of the selected optimization variables are presented in Tab. 2.

Tab. 1 Design specifications of the machine

Item	Requirement
Rated speed/(r/min)	1 500
Rated current/A	6
Outer diameter/mm	136
Stack length/mm	40
Air gap/mm	0.5
Output torque/(N • m)	≥6
Torque ripple(%)	≤10

Tab. 2 Design parameters of the machine

Item	Initial value	Variation range
Pole opening angle *ARC*/(°)	10	[8-12]
Magnet width *PMH*/mm	5.2	[4.5-6.1]
Air magnetic barrier angle *AN*/(°)	2	[1.0-3.0]
First shift angle SW_1/(°)	0	[2.0-4.0]
Second shift angle SW_2/(°)	0	[1.0-2.0]
Distance between magnet and rotor outer diameter R_d/mm	0.2	[0.1-0.3]
Slot opening width B_{S0}/mm	0.8	[0.6-1.0]
Slot wedge maximum width B_{S1}/mm	2.2	[2.0-2.4]

3 Deterministic optimization design

When the initial machine model is established, some variables are supposed to be optimized to meet the design requirements. Fig. 3 depicts the overall process of deterministic optimization design. In general, the process includes four parts.

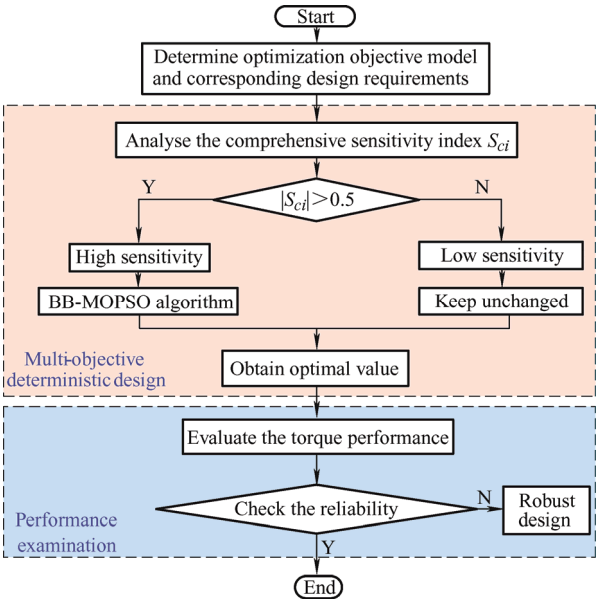

Fig. 3 Overall flowchart of the deterministic optimization design

First, according to the torque performance requirements, the optimization objective model and corresponding design requirements are determined.

Next, the sensitivity analysis method is used to evaluate the effects of each design variable on the optimization objectives. Here, the comprehensive sensitivity coefficient (S_c) is calculated to classify the design variables into different levels.

Then, suitable optimization methods are adopted to deal with variables of different sensitivity levels. For high-sensitivity design variables, the BB-MOPSO algorithm is used to find the optimal solution via the response surface (RS) equation. For low-sensitivity design variables, the values are kept unchanged.

Finally, the optimal solution must be validated by ensuring that the result corresponds to the design specifications. Additionally, the reliability of the deterministic optimization results must be checked to determine whether robust optimization is needed.

3.1 Determination of optimization objective model

For permanent magnet (PM) machines, a high

average torque and low torque ripple are the key performance aspects. Hence, the average torque and torque ripple are selected as optimization objectives.

When multiple optimization objectives are determined, the comprehensive optimization objective function is introduced to assess the overall torque performance. According to the idea of the weight, each independent optimization objective is multiplied by a weight coefficient (λ) to reflect its relative importance. The overall optimization objective function can be defined as [28]

$$\begin{cases} G_{\min}(x_i) = \lambda_1 \dfrac{T_{rip}(x_i)}{T_{rip\_0}} + \lambda_2 \dfrac{T_{avg\_0}}{T_{avg}(x_i)} \\ \lambda_1 = 0.5 \quad \lambda_2 = 0.5 \end{cases} \tag{1}$$

where $G(x_i)$ is the overall optimization objective function, which aims to find the minimum value during the optimization process. T_{rip_0} and T_{avg_0} represent the initial values of the torque ripple and average torque, respectively. λ_1 and λ_2 are the weight coefficients of the torque ripple and average torque, respectively. In this study, λ_1 and λ_2 are set as 0.5 to combine a high average torque and low torque ripple owing to the rotor magnet shifting and air barrier design.

Furthermore, regarding the constraint conditions, the design variables must satisfy the design variations presented in Tab. 2, and the electromagnetic performance must be improved. The corresponding expression is

$$\text{s.t.:} \begin{cases} \min x_i \leqslant x_i \leqslant \max x_i \\ g_1(x_i) = 6 - T_{av} \leqslant 0 \\ g_2(x_i) = T_{rip} - 10 \leqslant 0 \end{cases} \tag{2}$$

where x_i represents the design variables, and $g_1(x_i)$ and $g_2(x_i)$ are the average torque and torque ripple constraint functions concerning the design variables.

3.2 Comprehensive sensitivity analysis

The comprehensive sensitivity analysis method was used to evaluate the effects of different design variables on the multiple optimization objectives without interaction [29]. For clear assessment, a mathematical index called the sensitivity coefficient was introduced to identify the different contributions from each design variable. The simple sensitivity coefficient is given as [30-32]

$$S = \frac{V(E(y|x_i))}{V(y)} \tag{3}$$

where $E(y|x_i)$ represents the expected value of y changed by x_i when the initial values of the other design variables remain unchanged. $V(E(y|x_i))$ represents the variance of $E(y|x_i)$, and $V(y)$ represents the variance of y when x_i is combined with other parameters.

For multiple optimization objectives, the sensitivity analysis method should reflect the overall effects on all the optimization objectives. Therefore, the comprehensive sensitivity coefficient is introduced to assess and classify the design variables. According to the weight coefficient (λ), the comprehensive sensitivity coefficient (S_c) can be obtained as follows

$$S_c(x_i) = \lambda_1 S_{Tav}(x_i) + \lambda_2 S_{Trip}(x_i) \tag{4}$$

where $S_{Tav}(x_i)$ is the simple sensitivity coefficient of the i^{th} design variable for the average torque, and $S_{Trip}(x_i)$ is the simple sensitivity coefficient of the i^{th} design variable for the torque ripple. λ_1 and λ_2 are the weight coefficients of the average torque and torque ripple, respectively, which are both set as 0.5.

Fig. 4 shows the results of the sensitivity analysis. The sign of the sensitivity coefficient (positive or negative) is determined by the influence of the design variable on the machine performance. For example, if five evenly spaced values within the variation range of the design variable are selected, the five responses can be obtained, and the performance variation tendency can be determined. When the performance is promoted or enhanced, the sign of the sensitivity coefficient is positive, whereas a negative sign of the sensitivity coefficient indicates reduced performance. The absolute value of the sensitivity coefficient represents the degree of influence on the optimization objectives. *ARC* has the most significant effect on the torque performance when the volume of the PM remains unchanged. SW_1 and SW_2 have positive effects on the torque ripple. *AN* has a positive effect on the average torque and a negative effect on the torque ripple, and this conflict makes it difficult to select a suitable value.

Finally, the comprehensive sensitivity of the parameters is evaluated according to Eq. (4), and the

parameters are classified into two levels. The specific results are presented in the Tab. 3. Therefore, the design space is significantly reduced to improve the optimization efficiency.

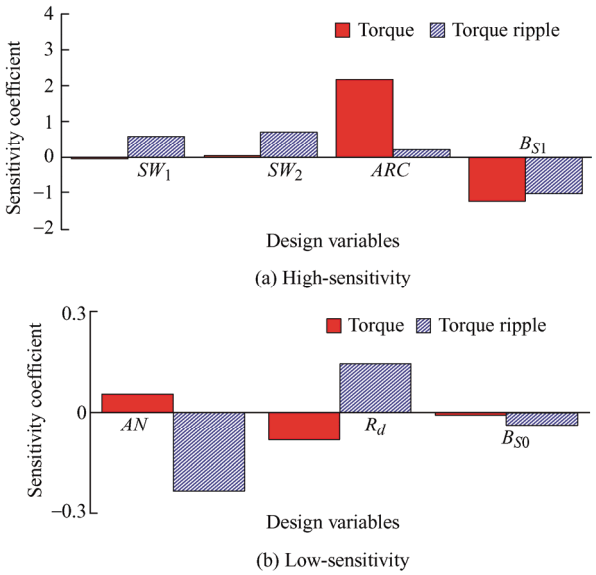

Fig. 4 Results of the sensitivity analysis

Tab. 3 Comprehensive sensitivity coefficient and classification

Level	Item	Comprehensive sensitivity coefficient
High-sensitivity	SW_1	0.61
	SW_2	0.71
	ARC	1.98
	B_{S1}	1.00
Low-sensitivity	AN	0.15
	R_d	0.11
	B_{S0}	0.02

3.3 Multi-level optimization design

The response surface method (RSM) is adopted to optimize the high-sensitivity design variables [33]. The reasonable experimental design and the multiple regression equation are adapted to fit the function relationship between design variables and objectives.

Among the numerous experimental design methods, the Box-Behnken design (BBD) method has been widely used [16, 34] and is effective for obtaining the representative cases needed for the RS equation. The distribution of sample points of the three design variables is illustrated in Fig. 5. Each factor has three levels encoded by –1, 0, and +1, respectively, where +1 and –1 represent the high and low variation values and 0 is the center point. The finite-element method (FEM) is used to obtain the optimization objective results based on the representative cases needed in BBD.

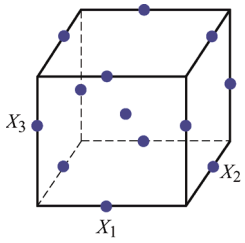

Fig. 5 Distribution of sample points in BBD

Afterward, the RSM is employed to develop the analytical function relationship between variables and response values, and the machine model is replaced with a mathematical model. The response model concerning the average torque and torque ripple can be expressed as

$$Y = \beta_0 + \sum_{i=1}^{k} \beta_i x_i + \sum_{i=1}^{k} \beta_{ii} x_i^2 + \sum_{i=1,i<j}^{k} \beta_{ij} x_i x_j + \varepsilon \quad (5)$$

where Y represents the predicted value of a design objective, and k represents the index of the design variables. In this study, k=4.

To verify the effectiveness of the established RS equation, it is essential to analyze the probability of failure (POF) of the equation [35], for which the multiple correlation coefficient R^2 and the root-mean-square error (*RMSE*) are deemed as the two basic criteria. R^2 is used to test how close the fitting model is to the actual performance. The *RMSE* is adopted to illustrate the error of the model, and it is given as follows

$$RMSE = \sqrt{\frac{1}{N}\sum_{i=1}^{N}(y_i - \hat{y}_i)^2} \quad (6)$$

where y_i represents the simulated value, $\hat{y}_i$ represents the predicted value of the established equation, and N represents the number of experimental sample points.

In general, when R^2 is closer to 1 and the *RMSE* is closer to 0, the reliability of the model is higher [16]. When R^2 and *RMSE* are undesirable, the significance test and the variance must be analyzed to adjust the adaptability of the RS equation. Tab. 4 presents the R^2 and *RMSE* results for the established torque and torque ripple equation. As shown, R^2 is close to 1, and the *RMSE* is close to 0. Thus, the RS equations are effective.

Tab. 4 R^2 and *RMSE* for established torque and torque ripple equation

Items	R^2	*RMSE*
Torque	0.999 6	0.009 6
Torque ripple	0.977	0.019

For four high-sensitivity design variables, 29 sample points are needed to establish the RS equation concerning the average torque and torque ripple, which are also viewed as training points. Then, the RSM results for the FEM and RS equations are compared and analyzed, as shown in Fig. 6. The torque equation fits well with the 29 sample points, whereas several errors exist for the torque ripple equation. Fortunately, these errors are within 15%, which are acceptable. Thus, the RS equations are valid.

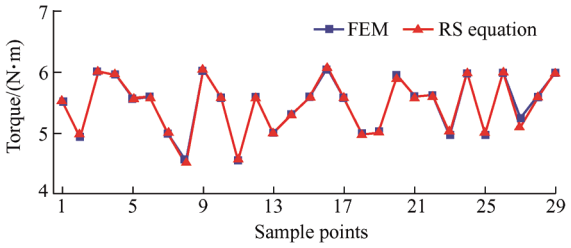

(a) Average torque

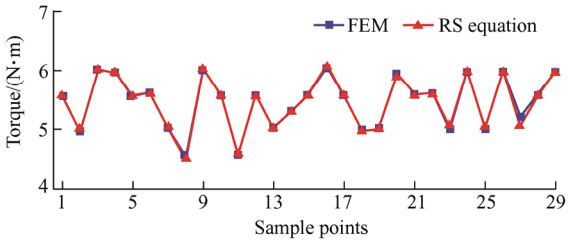

(b) Torque ripple

Fig. 6 Results for the FEM and RS equations

Finally, the BB-MOPSO algorithm is introduced to achieve the compromise solution [36-38], which combines the barebones particle swarm with multi-objective optimization design to resolve the conflicts between multiple variables and objectives. The BB-MOPSO algorithm has fewer control parameters, has a higher collection speed, and can better solve high-dimensional problems than other optimization algorithms. Additionally, the Pareto front has a good distribution, which is more conducive to selecting the best solution among many Pareto solutions. The BB-MOPSO algorithm can be divided into the following five parts, and a flowchart is presented in Fig. 7.

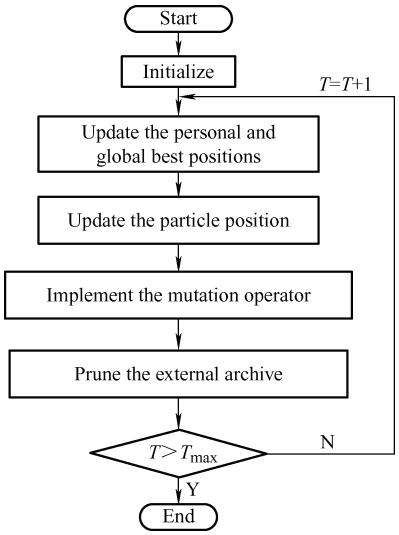

Fig. 7 Flowchart of the BB-MOPSO algorithm

Step 1: Initialize the corresponding parameters. The size of the swarm (*Ns*), the maximum capacity of the archive (*Na*), and the maximum number of iterations ($T_{\max}$) are first generated. Then, the initial value of the personal best position is defined as the particle itself. Afterward, the iteration steps are run circularly to find the optimal set of the optimization problem until $T_{\max}$ is reached. In this study, *Ns* is set to 50, *Na* is 100, and $T_{\max}$ is 500.

Step 2: Update the personal and global best positions. The personal best position (P_{best}) is the best position achieved by the particle thus far. When the current position is better than the position in the memory, the P_{best} is replaced with the current position and vice versa. The update equation is as follows

$$Pb_i(t+1)=\begin{cases} Pb_i(t) & F(Pb_i(t)) \prec F(x_i(t+1)) \\ x_i(t+1) & \text{Otherwise} \end{cases} \tag{7}$$

where $x_i(t)$ represents the position of the i^{th} particle in the swarm.

The global best position (G_{best}) represents the best solution among the neighbor solutions obtained thus far. Considering the conflicts between multiple objectives, an external archive is adapted to store the nondominated solutions with the maximum capacity. Then, the crowding distance is introduced to estimate the diversity of nondominated solutions. In this study, two optimization objectives are considered, and the crowding distance can be calculated using the average side length of the cuboid formed by two adjacent solutions. The probability of getting G_{best} increases with the crowding distance. Consequently, the G_{best}

can be acquired when the crowding distance can be achieved in each iteration.

Step 3: The particle's position is updated. The corresponding expression is as follows

$$x_{i,j}(t+1)=\begin{cases} N\left(\dfrac{rPb_{i,j}(t)+(1-r)Gb_{i,j}(t)}{2},\left|Pb_{i,j}(t)-Gb_{i,j}(t)\right|\right) & U(0,1)<0.5 \\ Gb_{i,j}(t) \quad \text{Otherwise} \end{cases} \tag{8}$$

where r represents a random number in the range of [0, 1]. $Pb_{ij}(t)$ and $Gb_{ij}(t)$ represent the personal best position and global best position, respectively.

Step 4: Although the particle swarm optimization has a high convergence speed, the algorithm may converge to a false Pareto front. Thus, the mutation parameter (α) is proposed to control the decreasing speed of the mutation probability and enhance the search capability with the action range varying over time. At the initial state of iteration, all particles are affected, and with increasing iterations, the function of α is reduced; the specific expression is $\exp(-\alpha*T/T_{\max})$. In this study, α is set as 2.

Step 5: To obtain an ideal setting at the end of the algorithm and the desired G_{best}, the external archive with maximal capacity is adopted to retain the nondominated solutions and needs to be pruned. When the archive reaches its maximal capacity, the archive size must be reduced using the crowding distance.

Considering that even small variations to high-sensitivity design variables may significantly affect the optimization objectives, the accurate and effective BB-MOPSO algorithm based on the RS equation and constraint conditions is adopted. The BB-MOPSO algorithm can only be used to find the minimum value of the RS equation, and the minus sign is added for the average torque. As shown in Fig. 8, there is a discrepancy between the minimum torque ripple and the maximum average torque. The red points represent the Pareto front, where the compromise solution is obtained.

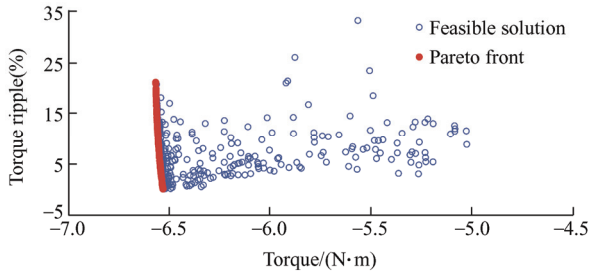

Fig. 8 Pareto front of the BB-MOPSO algorithm in deterministic design

For low-sensitivity level design variables, the mutual influence between variables and objectives can be neglected, and the values remain unchanged.

3.4 Optimization results and reliability verification

According to Eq. (1), the best point can be found from the Pareto front. Tab. 5 presents the deterministic optimization design results. After optimization, the average torque is changed from 5.9 N • m to 6.7 N • m, increasing by nearly 14%, and the torque ripple is changed from 23.3% to 3.6%, decreasing by >85%. The electromagnetic performance is significantly improved.

Tab. 5 Optimization results for deterministic design

Items	Initial results	Optimal results
SW_1	0	2.8
SW_2	0	1.4
ARC	10	11.5
B_{S1}	2.2	2
B_{S0}	0.8	0.8
R_d	0.2	0.2
AN	2	2
T_{av}/(N • m)	5.9	6.7
T_{rip} (%)	23.3	3.6

However, the optimal values of the design variables are often achieved at the extreme points, which are highly sensitive to the variable fluctuation, and the reliability of the optimal results may be affected. Consequently, the POF is considered as an evaluation metric to verify the reliability of the products when noise factors occur. According to the multiplication theorem in statistics, the POF can be defined as [39]

$$P_f = p(g(x)>0) \leqslant P^{\mathrm{u}} \tag{9}$$

where P_f represents the POF, and P^{u} represents the upper bound.

According to Eq. (9), the POF in deterministic design is 77.2% for average torque and 60% for torque ripple, and the integral POF is 46%. In the actual

production process, this is unacceptable. Therefore, it is necessary to conduct a robust design.

4 Robust optimization design

Although the electromagnetic performance is significantly enhanced, the values of the design variables are often achieved at the boundaries of design variations, which are viewed as peak points mathematically. However, manufacturing tolerances are unavoidable in mass production, making the performance highly sensitive and unstable. In Fig. 9, the first point represents the deterministic solution, and the second point represents the robust solution. The performances are almost identical. However, when noise factor Δx occurs, the variation in the deterministic design Δf_1 is larger than that in the robust design Δf_2, which is unacceptable. Hence, the robust optimization design is indispensable.

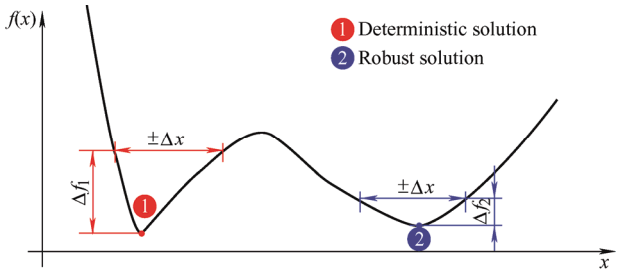

Fig. 9 Differences between deterministic and robust designs

The robust optimization design can be divided into the following three steps, as shown in Fig. 10.

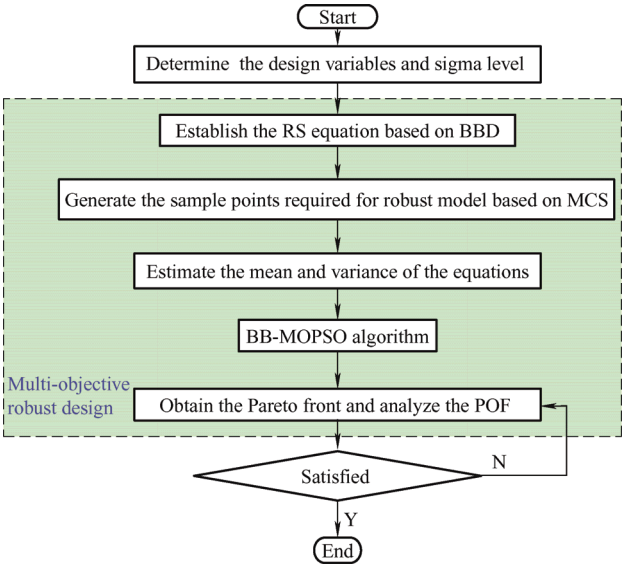

Fig. 10 Flowchart of the robust optimization design

Step 1: The design variables and optimization objectives are chosen. The sign level is a statistical measure of quality to represent the manufacturing process, which must be determined.

Step 2: The optimization objectives and constraint equations are set up according to the RSM. Afterward, the DFSS and MCS are adopted to estimate μ and σ. Thus, the robust design model and boundaries can be set up.

Step 3: The BB-MOPSO algorithm is used to optimize the robust design model and find the optimal solution. Finally, the torque performance and reliability are verified.

4.1 Robust design model

The deterministic optimization model given by Eqs. (1)-(2) does not cover the unavoidable manufacturing tolerances and noise factors. For solving these problems, a robust model based on the DFSS is essential, where the mean values (μ) and standard deviations (σ) of all the design variables and optimization objective equations are considered. The core of the robust design is to improve the mean values and reduce the standard deviations of the robust model in a mathematical sense, implying that the machine performance is improved while the fluctuations caused by noise factors are reduced in a manufacturing sense.

First, SW_1, SW_2, ARC, and B_{S1} are selected as design variables considering their high sensitivity to the machine performance. According to previous research, these design variables are assumed to follow a normal distribution. For the possible application in electrical vehicles, a high average torque and low torque ripple are selected as optimization objectives as well. Thus, the robust models can be expressed as follows [40-42]

$$\min: f_{\min}(x_i)=\lambda_1\mu\left(\frac{T_{rip}(x_i)}{T_{rip\_0}}\right)+\lambda_2\mu\left(\frac{T_{avg\_0}}{T_{avg}(x_i)}\right) \quad i=1,\cdots \tag{10}$$

$$\text{s.t.:}\begin{cases} g[\mu_f(x),\sigma_f(x)]\leqslant 0 & m=1,2 \\ x_l+n\sigma_{xi}\leqslant\mu_{xi}\leqslant x_u-n\sigma_{xi} & i=1,\cdots,4 \\ LSL\leqslant\mu_f\pm n\sigma_f\leqslant USL \end{cases} \tag{11}$$

where $T_{rip}(x_i)$ and $T_{avg}(x_i)$ represent the torque ripple and average torque function concerning four design variables, which can be established using the RSM. Although the relevant equations have been fitted before, owing to the different range of variation, the

equations must be refitted to obtain a satisfactory accuracy. The constraint functions concerning the two optimization objectives are also constructed using the RSM, and the variables are highly sensitive. The sample points needed to establish μ and σ are adopted in the MCS and DFSS. x_l and x_u represent the boundaries of the design variables, σ_{xi} represents the standard deviation of the design variables, and n represents the sigma level, which is equivalent to a probability in a standard normal distribution. *LSL* and *USL* are the lower and upper specification limits, respectively.

The manufacturing variations of the design variables may be small; thus, 5% is selected as the variation boundary. Additionally, the design variables are deemed to follow the normal distribution $N(x_i, \sigma_{xi}^2)$, where x_i represents the optimal value obtained in deterministic design. $\sigma_{xi}=\Delta x_i/3$, where Δx_i represents the manufacturing tolerance and is equivalent to 5% of x_i. Then, according to the preferred sigma rating and the variation range, the design variables can be calculated.

The sigma rating is used to estimate the yield or the number of defects per million opportunities (DPMO), which refers to the ratio of the number of the products violating the design constraints to the total number of products when the surrogate models are precisely constructed [43-44]. Tab. 6 presents the sigma levels for the percent variation and DPMO. When the design variables are normally distributed, the results in Tab. 6 can be employed to measure the DPMO of the products. Taking 4σ as an example, the required probability is 99.993 7% or 63 DPMO, which is acceptable in the short term. However, a 1.5σ shift is vital in the long term, considering the actual manufacturing and engineering aspects. The DPMO of 4σ is 6 200, which is insufficient in manufacturing. Consequently, 6σ is often preferred to satisfy the short- and long-term manufacturing requirements, for which the DPMO is 0.002 and 3.4, respectively.

Tab. 6 Sigma levels for the percent variation and DPMO

Sigma level	Percent variation	DPMO (short term)	DPMO (long term–1.5σ shift)
$\pm1\sigma$	68.26	317 400	697 700
$\pm2\sigma$	95.46	45 400	308 733
$\pm3\sigma$	99.73	2 700	66 803
$\pm4\sigma$	99.993 7	63	6 200
$\pm5\sigma$	99.999 943	0.57	233
$\pm6\sigma$	99.999 999 8	0.002	3.4

MCS is a computational approach based on probability and statistical theory, which is employed to solve many uncertainty problems and calculate the μ and σ in Eqs. (10)-(11). In this study, 10 000 sample points were adopted to estimate the statistic characteristic.

According to the results of the DFSS and the MCS, the robust model is shown in Fig. 11. There are conflicts between the average torque and torque ripple. With an increase in *ARC*, the average torque increased slightly, while the torque ripple first decreased and then increased. It is important to select the optimal value of *ARC* to achieve both high average torque and low torque ripple.

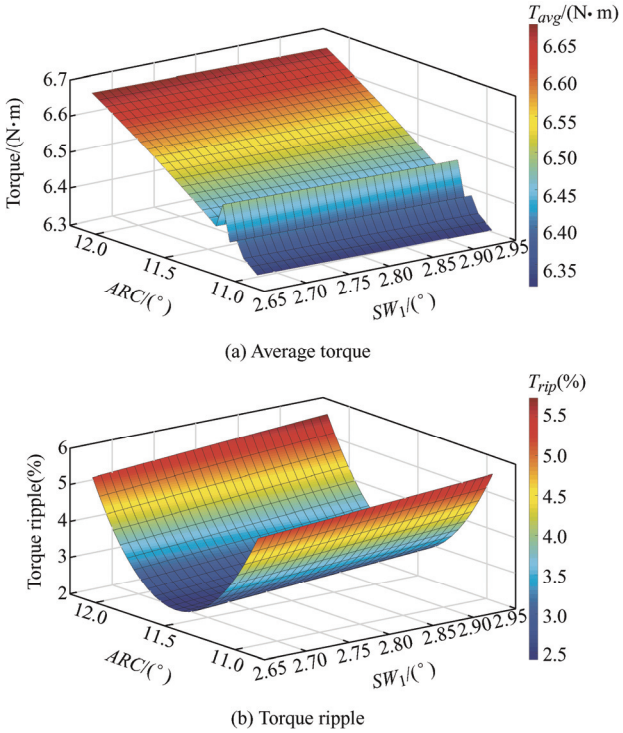

Fig. 11 Results of a robust model for *ARC* and SW_1

4.2 BB-MOPSO algorithm for robust design model

Because of the conflicts between design variables and optimization objectives in robust design, the BB-MOPSO algorithm was adopted to obtain the Pareto front and achieve the compromise solution. The results are presented in Fig. 12. The variation was narrower than that for the deterministic design in Fig. 8. Tab. 7 presents the final results. As shown, after the robust design, the average torque remained the same, while the torque ripple was increased

from 3.6% to 4.5%. The electromagnetic performance was almost identical, but according to Eq. (9), the POFs of the average torque and torque ripple were reduced to zero.

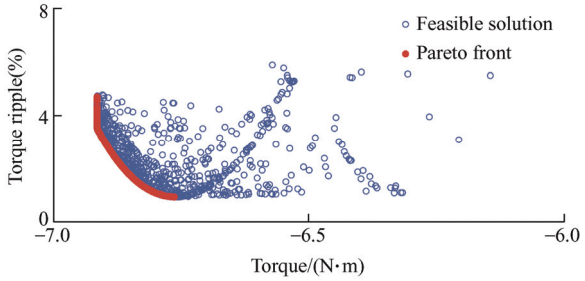

Fig. 12 Pareto front of the BB-MOPSO algorithm in a robust design

Tab. 7 Optimization results of robust design

Items	Deterministic results	Robust results
SW_1	2.8	2.7
SW_2	1.4	1.8
ARC	11.5	11.58
B_{S1}	2	1.9
T_{av}/(N • m)	6.7	6.7
T_{rip} (%)	3.6	4.3

5 Verification of robust optimization design

The electromagnetic performance and robustness of the ISPM machine were compared after the robust design, including the no-load performance, torque characteristics, and POF.

5.1 No-load back electromotive force (EMF)

The no-load back-EMF waveform is an important standard for measuring the machine performance and can influence the torque ripple, vibration, and noise. The waveforms for the initial, deterministic, and robust optimization models are shown in Fig. 13. The waveforms of the optimization models are more sinusoidal than that of the initial model.

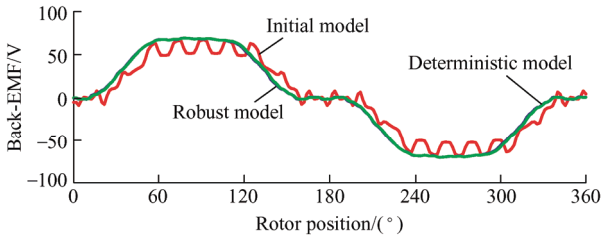

(a) Waveform

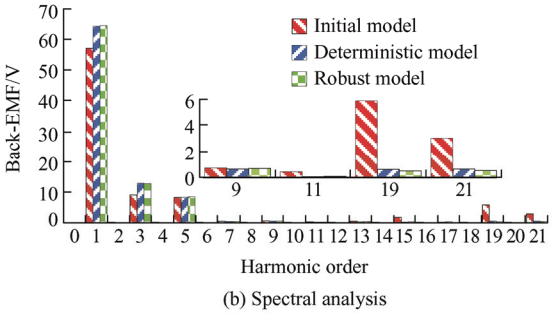

(b) Spectral analysis

Fig. 13 Comparison of the no-load back-EMF

A five-phase machine was adopted in this study. The key orders affecting torque ripple were the 9th, 11th, 19th, and 21st. After optimization, all the key orders were reduced nearly to zero, leading to the low torque ripple.

5.2 Cogging torque

Because cogging torque is related to the torque ripple, its waveforms were compared as well. As shown in Fig. 14, the peak-to-peak values of the cogging torque were significantly reduced—from 1 346 mN •m to 85.8 mN • m in the deterministic design and 76.8 mN • m in the robust design—indicating a reduction of up to 90%. Consequently, the torque ripple was reduced as well.

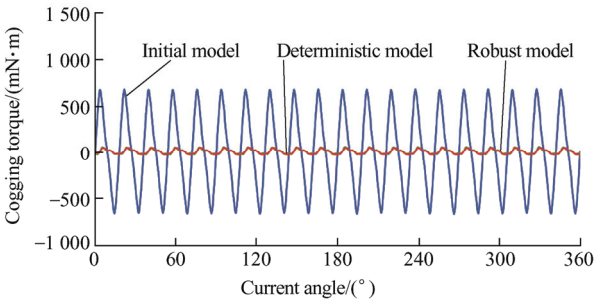

Fig. 14 Comparison between cogging torque

5.3 Average torque and torque ripple

Fig. 15a presents the optimization results for the average torque and torque ripple. For the deterministic design, the average torque was increased from 5.9 N •m to 6.7 N •m, while the torque ripple was reduced from 23.3% to 3.6%; thus, the electromagnetic performance was significantly improved. On this basis, the robust design was employed, and the average torque was maintained while the torque ripple increased slightly. Furthermore, a spectral analysis was performed, as shown in Fig. 15b. Both the fundamental amplitudes of

the deterministic and robust designs were improved, and the 20th-order harmonic amplitude was reduced to zero, which explains the reduction in the torque ripple.

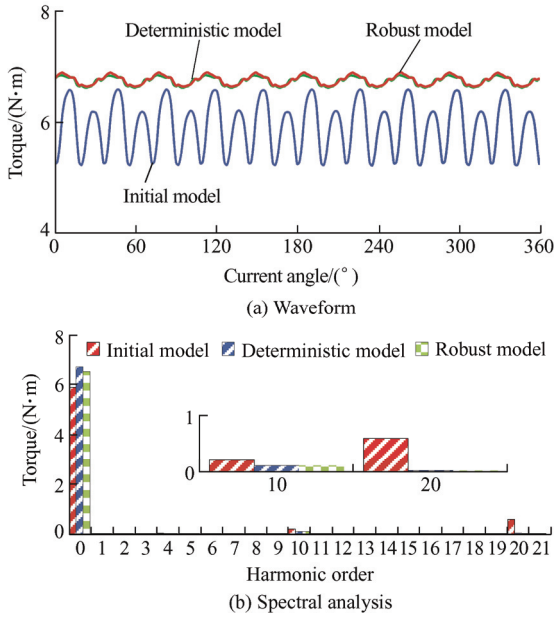

Fig. 15 Comparison of the torque performance

5.4 POF

The POF is a criterion for evaluating the reliability of the proposed machine in mass production. A comparison of the POF results is shown in Fig. 16. The distributions of the average torque and torque ripple in the robust design were narrower than those in the deterministic design. Additionally, the failure areas of the products violating the design requirements were reduced to zero, and the POF in the robust design was zero as well. Thus, the robustness was significantly improved.

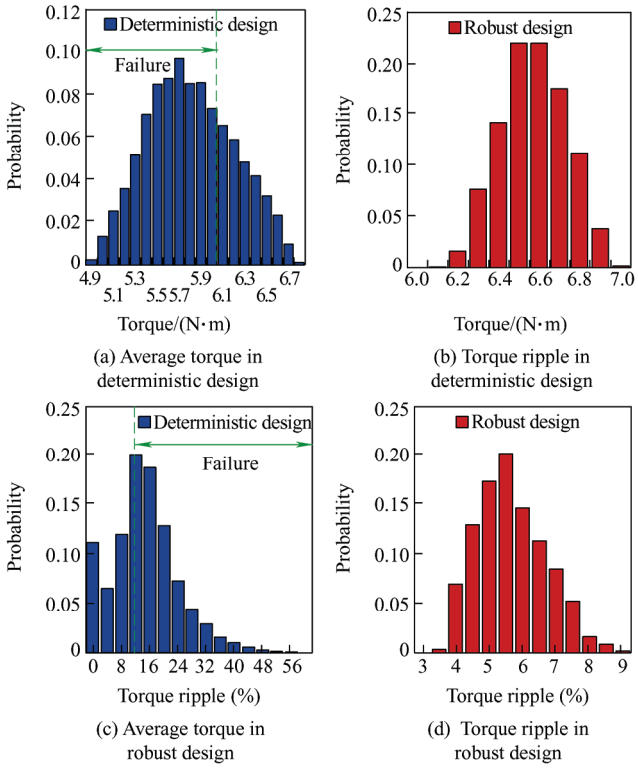

Fig. 16 Comparison of the POFs

6 Experimental verification

The optimized ISPM machine was manufactured and tested to validate the proposed optimization design method. The experimental platform is shown in Fig. 17.

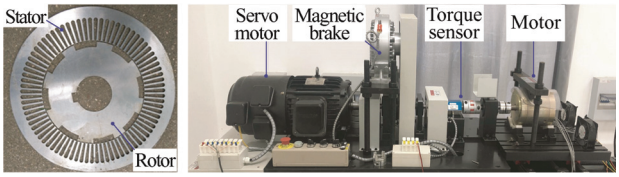

Fig. 17 Experimental platform

The measurement and FEM results for the phase back-EMF waveforms of the proposed ISPM machine at 1 500 r/min are presented in Fig. 18a. As shown, the measurement and simulation results differed slightly. To investigate this, a spectral analysis of the phase back-EMF was performed, as shown in Fig. 18b. The fundamental values of the back-EMF were identical between the measurement and simulation results. The main harmonic orders creating the torque ripple were the 9th, 11th, 19th, and 21st, the amplitudes were all reduced to less than 1 V. However, the measured harmonic amplitudes were larger than the FEM results, which may have contributed to the deviation in the torque ripple.

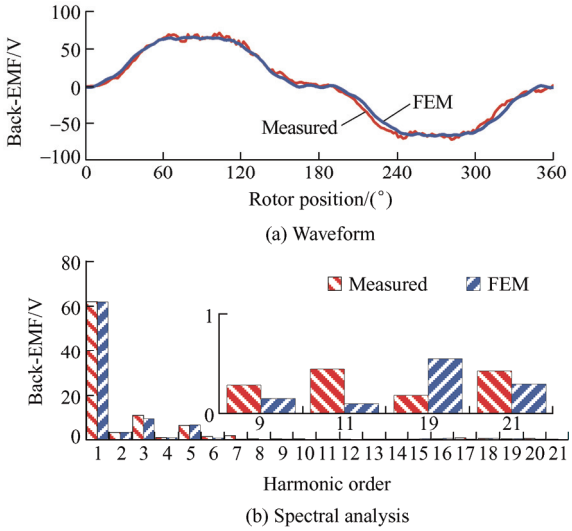

Fig. 18 Comparison of the no-load back-EMF between the FEM and measurement results

The instantaneous torque at 30 r/min is presented in Fig. 19a. Here, the current amplitude was 6 A, and the current angle was 35° . Double closed-loop control was adopted. The measurement and simulation results are compared in Fig. 19b. In the experiment, the average torque was 6.1 N •m, and the peak-to-peak value was 0.7 N • m. In the simulation, the average torque was 6.7 N • m, and the peak-to-peak value was 0.3 N • m. For a clear explanation, a spectral analysis was performed, as shown in Fig. 19c. The measurement result for the 2nd torque ripple was larger in the experiment. The main harmonic orders affecting the average torque were the 10th and 20th. In the experiment, the amplitude of 10th-order harmonic was relatively small, and that of 20th-order harmonic exhibited almost no variation. Consequently, the average torque was lower in the experiment than in the FEM. In summary, the slight eccentricity of the experimental platform and the loss of average torque led to the deviation of the torque ripple.

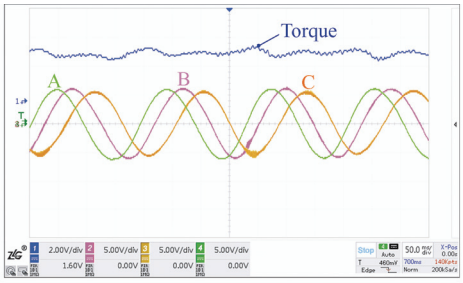

(a) Instantaneous torque and current at a current angle of 35°
(2 N·m/div，5 A/div)

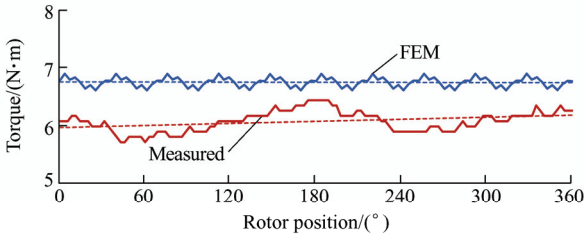

(b) Comparison between measured and simulated torques

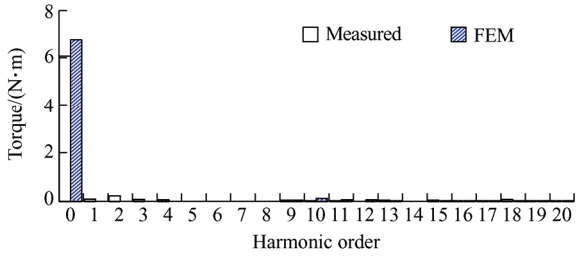

(c) Spectral analysis of measured and simulated torques

Fig. 19 Measured torque performance at a current of 6 A

The torque performance for different current angles is presented in Fig. 20. The average torques were almost identical between the experiment and FEM, and the maximum torque was obtained at a current angle of 35° . The slight eccentricity of the experimental platform may contributed to the deviation in the torque ripple. Thus, the optimized ISPM machine can realize a high average torque and low torque ripple.

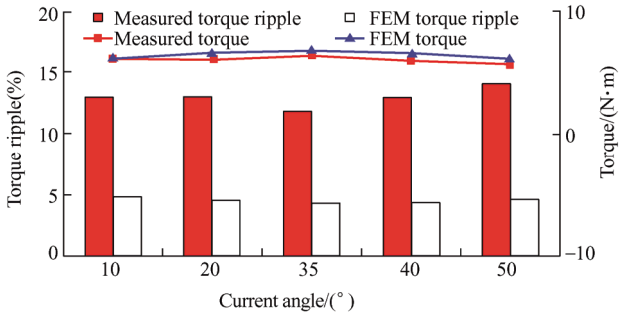

Fig. 20 Instantaneous torque for different current angles

7 Conclusions

A multi-objective robust optimization design method to be applied after deterministic design is proposed. The appropriate methods were skillfully employed in this study. First, the machine is optimized according to the deterministic design. Then, considering the unavoidable noise factors, DFSS and MCS are employed in the robust design to enhance the reliability of the proposed machine. According to a comparison between initial and optimized results, the proposed method improved not only the electromagnetic performance but also the robustness of the machine.

References

[1] Q Chen, G Xu, G Liu, et al. Torque ripple reduction in five-phase interior permanent magnet motors by lowering interactional MMF. *IEEE Trans. Ind. Electron*., 2018, 65(11): 8520-8531.

[2] P Chen, K Hu, Y Lin, et al. Development of a prime mover emulator using a permanent-magnet synchronous motor drive. *IEEE Trans. Power Electron*., 2018, 33(7): 6114-6125.

[3] S K Lee, G H Kang, J Hur. Finite element computation of magnetic vibration sources in 100 kW two fractional-slot interior permanent magnet machines for a ship. *IEEE Trans. Magn*., 2012, 48(2): 867-870.

[4] J Zheng, W Zhao, J Ji, et al. Sleeve design of

permanent-magnet machine for low rotor losses. *Chinese Journal of Electrical Engineering*, 2020, 6(4): 86-96.

[5] J Gan, K Chau, C Chan, et al. A new surface-inset permanent-magnet brushless DC motor drive for electric vehicles. *IEEE Trans. Magn.*, 2000, 36(5): 3810-3818.

[6] W Zhao, T Lipo, B Kwon. Optimal design of a novel asymmetrical rotor structure to obtain torque and efficiency improvement in surface inset PM motors. *IEEE Trans. Magn.*, 2015, 51(3): 8100704.

[7] Z Ling, J Ji, T Zeng, et al. Design optimization and comparison of linear magnetic actuators under different topologies. *Chinese Journal of Electrical Engineering*, 2020, 6(1): 41-51.

[8] G Liu, X Du, W Zhao, et al. Reduction of torque ripple in inset permanent magnet synchronous motor by magnets shifting. *IEEE Trans. Magn.*, 2017, 53(2): 8100713.

[9] Y Jung, M Lim, J Jeong, et al. Torque ripple reduction of IPMSM applying asymmetric rotor shape under certain load condition. *IEEE Trans. Energy Convers.*, 2018, 33(1): 333-340.

[10] L Huang, J Feng, S Guo, et al. Rotor shaping method for torque ripple mitigation in variable flux reluctance machines. *IEEE Trans. Energy Convers.*, 2018, 33(3): 1579-1589.

[11] G Liu, G Xu, W Zhao, et al. Improvement of torque capability of a permanent-magnet motor by using hybrid rotor configuration. *IEEE Trans. Energy Convers.*, 2017, 32(3): 953-962.

[12] X Du, G Liu, Q Chen, et al. Optimal design of an inset PM motor with assisted barriers and magnet shifting for improvement of torque characteristics. *IEEE Trans. Magn.*, 2017, 53(11): 8109204.

[13] G Liu, Z Lin, W Zhao, et al. Third harmonic current injection in fault-tolerant five-phase permanent-magnet motor drive. *IEEE Trans. Ind. Electron*., 2018, 33(8): 6970-6979.

[14] Y Guo, J Si, C Gao, et al. Improved fuzzy-based Taguchi method for multi-objective optimization of direct-drive permanent magnet synchronous motors. *IEEE Trans. Magn.*, 2019, 55(6): 8102204.

[15] F Dong, J Song, J Zhao, et al. Multi-objective design optimization for PMSLM by FITM. *IET Electr. Power Appl.,* 2018, 12(2): 188-194.

[16] W Zhao, A Ma, J Ji, et al. Multi-objective optimization of a double-side linear vernier PM motor using response surface method and differential evolution. *IEEE Trans. Ind. Electron*., 2020, 67(1): 80-90.

[17] L Xu, W Zhao, G Liu, et al. Design optimization of a spoke-type permanent-magnet vernier machine for torque density and power factor improvement. *IEEE Trans. Veh. Technol.*, 2019, 68(4): 3446-3456.

[18] X Zhu, W Wu, L Quan, et al. Design and multi-objective stratified optimization of a less-rare-earth hybrid permanent magnets motor with high torque density and low cost. *IEEE Trans. Energy Convers.,* 2019, 34(3): 1178-1189.

[19] D Lee, A Yoon, S Sirimanna, et al. Impact of manufacturing tolerances on a low-reactance slotless PM synchronous machine. *IEEE Trans. Energy Convers.,* 2019, 35(1): 366-374.

[20] I Coenen, M Giet, K Hameyer. Manufacturing tolerances: Estimation and prediction of cogging torque influenced by magnetization faults. *IEEE Trans. Magn.*, 2012, 48(5): 1932-1936.

[21] M Zhou, X Zhang, W Zhao, et al. Influence of magnet shape on the cogging torque of a surface-mounted permanent magnet motor. *Chinese Journal of Electrical Engineering*, 2019, 5(4): 40-50.

[22] A Ortega, L Xu. Analytical prediction of torque ripple in surface-mounted permanent magnet motors due to manufacturing variations. *IEEE Trans. Energy Convers.,* 2016, 31(4): 1634-1644.

[23] J Qu, Y Liu, R Qu, et al. Experimental and theoretical research on cogging torque of PM synchronous motors considering manufacturing tolerances. *IEEE Trans. Ind. Electron*., 2018, 65(5): 3772-3783.

[24] G Lei, T Wang, J Zhu, et al. System-level design optimization method for electrical drive systems-robust approach. *IEEE Trans. Ind. Electron*., 2015, 62(8): 4702-4713.

[25] P Putek, E Maten, M Gunther, et al. Variance-based robust optimization of a permanent magnet synchronous machine. *IEEE Trans. Magn.*, 2018, 54(3): 8102504.

[26] P Koch, R Yang, L Gu. Design for six sigma through robust optimization. *Struct. Multidiscip. Optim.*, 2004, 26: 235-248.

[27] Q Chen, Y Yan, G Xu, et al. Principle of torque ripple reduction in synchronous reluctance motors with shifted asymmetrical poles. *IEEE J. Emerg. Sel. Top. Power Electron.,* 2020, 8(3): 2611-2622.

[28] X Zhu, Z Xiang, L Quan, et al. Multimode optimization design methodology for a flux-controllable stator

permanent magnet memory motor considering driving cycles. *IEEE Trans. Ind. Electron.*, 2018, 65(7): 5353-5366.

[29] G Lei, C Liu, J Zhu, et al. Techniques for multilevel design optimization of permanent magnet motors. *IEEE Trans. Energy Convers.*, 2015, 30(4): 1574-1584.

[30] A Waqas, D Melati, A Melloni. Stochastic simulation and sensitivity analysis of photonic circuit through Morris and Sobol method. *Optical Fiber Communications Conference and Exhibition (OFC)*, 2017.

[31] B Assaad, K Benkara, S Vivier, et al. Thermal design optimization of electric machines using a global sensitivity analysis. *IEEE Trans. Ind. Electron*., 2017, 53(6): 5365-5372.

[32] X Sun, Z Shi, G Lei, et al. Analysis and design optimization of a permanent magnet synchronous motor for a campus patrol electric vehicle. *IEEE Trans. Veh. Technol.*, 2019, 68(11): 10535-10544.

[33] X Zhu, M Jiang, Z Xiang, et al. Design and optimization of a flux-modulated permanent magnet motor based on an airgap-harmonic-orientated design methodology. *IEEE Trans. Ind. Electron.*, 2020, 67(7): 5337-5348.

[34] G Bramerdorfer. Computationally efficient tolerance analysis of the cogging torque of brushless PMSMs. *IEEE Trans. Ind. Appl.*, 2017, 53(4): 3387-3393.

[35] J Li, D Xiu. Evaluation of failure probability via surrogate models. *J. Comput. Phys.,* 2010, 229(23): 8966-8980.

[36] Y Zhang, D Gong, Z Ding. A bare-bones multi-objective particle swarm optimization algorithm for environmental/economic dispatch. *Information Sciences*., 2012, 192: 213-227.

[37] M Ghasemi, S Ghavidel, M Ghanbarian, et al. Multi-objective optimal power flow considering the cost, emission, voltage deviation and power losses using a multi-objective modified imperialist competitive algorithm. *Energy*, 2014, 78: 276-289.

[38] B Qu, Y Zhu, Y Jiao, et al. A survey on multi-objective evolutionary algorithms for the solution of the environmental/economic dispatch problems. *Swarm Evol. Comput.,* 2018, 38: 1-11.

[39] V Rafiee, J Faiz. Robust design of an outer rotor permanent magnet motor through six-sigma methodology using response surface surrogate model. *IEEE Trans. Magn.*, 2019, 55(10): 8107110.

[40] C Jun, B Kwon. Process capability control procedure for electrical machines by using a six-sigma process for achieving six-sigma quality level. *IET Electr. Power Appl.,* 2017, 11(8): 1466-1474.

[41] M Islam, A Arafat, S Bonthu, et al. Design of a robust five-phase ferrite-assisted synchronous reluctance motor with low demagnetization and mechanical deformation. *IEEE Trans. Energy Convers.*, 2019, 34(2): 722-730.

[42] B Ma, G Lei, J Zhu, et al. Application-oriented robust design optimization method for batch production of permanent-magnet motors. *IEEE Trans. Ind. Electron*., 2018, 65(2): 1728-1739.

[43] G Bramerdorfer. Tolerance analysis for electric machine design optimization: Classification, modeling and evaluation, and example. *IEEE Trans. Magn.*, 2019, 55(8): 8106809.

[44] G Bramerdorfer. Effect of the manufacturing impact on the optimal electric machine design and performance. *IEEE Trans. Energy Convers*., 2020, 35(4): 1935-1943.

Gaohong Xu received B.Sc., M.Sc., and Ph.D. degrees from Jiangsu University, Zhenjiang, China, in 2009, 2011 and 2018, respectively, in Electrical Engineering.

She has been with Jiangsu University since 2018, where she is currently a Lecturer in School of Electrical Information Engineering. Her current research interests include computation of electromagnetic fields for permanent-magnet machine and electric machine design.

Zexin Jia received his B.S. degree in electrical engineering from Changshu Institute of Technology, Suzhou, China, in 2020. And he is currently working toward the M.Sc. degree in Electrical Engineering, Jiangsu University, Zhenjiang, China.

His research interests include optimization design and vibration noise simulation of permanent-magnet machine.

Wenxiang Zhao (M'08-SM'14) received the B.Sc. and M.Sc. degrees from Jiangsu University, Zhenjiang, China, in 1999 and 2003, respectively, and the Ph.D. degree from Southeast University, Nanjing, China, in 2010, all in Electrical Engineering.

He has been with Jiangsu University since 2003, where he is currently a Professor with the School of Electrical Information Engineering. From 2008 to 2009, he was a Research Assistant with the Department of Electrical and Electronic Engineering, University of Hong Kong, Hong Kong, China. From 2013 to 2014, he was a Visiting Professor with the Department of Electronic and Electrical Engineering,

University of Sheffield, Sheffield, UK. His current research interests include electric machine design, modeling, fault analysis, and intelligent control. He has authored and co-authored over 200 technical papers in these areas.

Qian Chen (M'16-SM'20) received the B.Sc. and Ph.D. degrees from Jiangsu University, Zhenjiang, China, in 2009 and 2015, respectively, in Electrical Engineering and Control Engineering.

He has been with Jiangsu University since 2015, where he is currently an Associate Professor in the School of Electrical Information Engineering. His current research interests include electric machine design, modeling, fault analysis, and intelligent control.

Guohai Liu (M'07-SM'15) received the B.Sc. degree from Jiangsu University, Zhenjiang, China, in 1985, and the M.Sc. and Ph.D. degrees from Southeast University, Nanjing, China, in 1988 and 2002, respectively, in Electrical Engineering and Control Engineering.

He has been with Jiangsu University since 1988, where he is currently a Professor, the Dean of the School of Electrical Information Engineering. From 2003 to 2004, he was a Visiting Professor with the Department of Electronic and Electrical Engineering, University of Sheffield, Sheffield, UK. His teaching and research interests include electrical machines, motor drives for electric vehicles and intelligent control. He has authored or co-authored over 200 technical papers and 4 textbooks, and holds 30 patents in these areas.